Swiss Journal of Geosciences (2019) 112:419–434
https://doi.org/10.1007/s00015-019-00342-5

U–Pb zircon provenance of Triassic sandstones, western Swiss Alps: implications for geotectonic history

Michael C. Wizevich[1] · Christian A. Meyer[2] · Ulf Linnemann[3] · Andreas Gärtner[3] · Benita-Lisette Sonntag[3] · Mandy Hofmann[3]

Received: 20 December 2018 / Accepted: 8 July 2019 / Published online: 6 August 2019

Abstract

The provenance of Triassic Vieux Emosson Formation, autochthonous sediments of the Aiguilles Rouges massif (External Alps), was determined from U–Pb ages of detrital zircons. In addition, two samples of Late Carboniferous sandstones from the Salvan-Dorénaz basin were included to extend the database of potential source rocks. Overall, age data from the four samples are largely comparable, each with a wide range of ages, indicating similar source rocks. The compositionally and texturally immature strata of the Vieux Emosson Formation suggest a local sediment source. However, not all detrital zircons can be accounted for by the ages of the local polymetamorphic pre-Mesozoic basement, which consists mainly of paragneiss, Ordovician orthogneiss and Late Carboniferous, Variscan-related, magmatic and sedimentary rocks. Ordovician zircons were common in the samples, but Late Carboniferous zircons were only abundant in one sample. Early Cambrian and older zircons were likely recycled from the paragneiss. Recycled zircons primarily represent Cadomian orogenic events (~ 550–650 Ma); older zircons are from eastern Gondwana and West African craton sources. Abundant late Cambrian (~ 500 Ma) and Silurian (~ 425 Ma) zircons likely represent Cadomian rifting and the magmatic events that produced the Ordovician orthogneiss, respectively. Permian zircons were only found in one Triassic sample, and are possibly related to magmatic activity associated with post-Variscan extension. The age data of the detrital zircons in the Triassic Vieux Emosson Formation and in the sandstones from the Late Carboniferous Salvan-Dorénaz basin indirectly dates the source rocks and for the first time confirms Cadomian basement in the Aiguilles Rouges massif. Source rocks for the Silurian, Permian, and to a lesser degree, late Cambrian zircons are not documented in the local basement, and either have been eroded away or are now located to the southeast beneath Penninic nappes.

Keywords Detrital zircon · U–Pb dating · Vieux Emosson Formation · Aiguilles Rouges massif · Triassic · Sediment provenance

1 Introduction

Sedimentological analysis demonstrated that sandstones of the Triassic autochthonous Vieux Emosson Formation were likely locally sourced from the Vindelician highland, the eastward extension of the Bohemian massif and a remnant upland of the Variscan orogenic belt, and transported

Editorial Handling: W. Winkler.

Electronic supplementary material The online version of this article (https://doi.org/10.1007/s00015-019-00342-5) contains supplementary material, which is available to authorized users.

✉ Michael C. Wizevich
wizevichmic@ccsu.edu

[1] Department of Geological Sciences, Central Connecticut State University, 1615 Stanley St, New Britain, CT 06050, USA

[2] Department of Environmental Sciences, University of Basel, Basel, Switzerland

[3] Museum für Mineralogie und Geologie, GeoPlasmaLab, Senckenberg Naturhistorische Sammlungen Dresden, Königsbücker Landstraße 159, D-01109 Dresden, Germany

northward in braided streams towards the Germanic Basin (Wizevich et al. 2019). Provenance analysis of the Vieux Emosson Formation provides an opportunity to learn how erosion of continental crust and sedimentation during the Triassic records the intricate geotectonic history of the Alpine External domain and assess paleogeographic reconstructions and tectonic models of the region.

The Vieux Emosson Formation lies unconformably on the Aiguilles Rouges crystalline massif, one of the External massifs in the Helvetic zone of the western Alps (Figs. 1 and 2). The External massifs are located near the southern edge of the Variscan basement of Europe that was not transported during Triassic-Jurassic extension and subsequent Alpine compression. The Aiguilles Rouges massif consists of a complex polymetamorphosed Cadomian-type (Neoproterozoic-Cambrian) basement with intercalated Ordovician orthogneisses that are cross cut by diverse Variscan (Hercynian) Late Carboniferous granitoids and intermontane sedimentary basins (Fig. 1b) (Capuzzo et al. 2003; von Raumer and Bussy 2004). A very low degree of Alpine overprint (von Raumer, 1969) of the basement allowed recognition of a Cadomian-type peri-Gondwana evolution with a high-grade metamorphic Variscan overprint (von Raumer et al. 1998; von Raumer et al. 2013).

This study utilizes LA–ICP–MS U–Pb dating of detrital zircons in the Vieux Emosson Formation to augment source area information obtained from outcrop and petrographic analyses (Fedo et al. 2003; Gehrels, 2011; Thomas 2011). Age dates of detrital zircons in the Vieux Emosson Formation provide confirmation, albeit indirect, of the hitherto poorly dated polyorogenic evolution of the Aiguilles Rouges basement. Two samples of Late Carboniferous sandstone from the Salvan-Dorénaz basin (Fig. 1) were also analysed for detrital zircons to extend the database of potential source rocks.

2 Geological setting

The primary basement blocks constituting the Aiguilles Rouge massif were emplaced during the Variscan orogeny as the rocks underwent severe compressional deformation, high-grade metamorphism, migmatization, plutonism and late-orogenic strike-slip tectonics (von Raumer 1998; von Raumer et al. 1999, 2009, 2013; Stampfli and Borel 2002). Associated with the strike-slip faulting was widespread magmatism and numerous pull-apart intermontane basins that developed in the Variscan crust and filled with thick sequences of continental sediments, such as the Late Carboniferous Salvan-Dorénaz basin in the Aiguilles Rouges massif (Fig. 1b) (von Raumer 1998; Capuzzo and Bussy 2000; Capuzzo and Wetzel 2004; von Raumer et al. 2009; Ballèvre et al. 2018). The Salvan-Dorénaz basin contains at least 1700 m of fluvial deposits, associated with fluvial systems that ranged from coarse-grained braided to sandy meandering to muddy anastomosing (Capuzzo and Wetzel 2004). U–Pb radiometric ages of volcanic deposits constrain the basin fill to Late Carboniferous (308–292 Ma) (Capuzzo and Bussy 2000; Capuzzo and Wetzel 2004). Late Caboniferous $^{40}Ar/^{39}Ar$ dates from detrital white mica indicate rapid basement exhumation and sediment derivation from local sources (Capuzzo and Wetzel 2004).

During the Triassic and Jurassic, the southern European margin rifted open to form Alpine Tethys. As the southern margin of Variscan basement domain fragmented, small ocean basins developed in the southern edge of the continent, the exact nature somewhat obscured by Alpine deformation (e.g., Stampfli and Borel 2002; Scheck-Wenderoth et al. 2008). In the study area, extension initiated in the Early Triassic, creating a complex network of faults and subsiding troughs (Ziegler 1982; Stampfli and Hochard 2009; de Graciansky et al. 2010). Differential thicknesses of Mesozoic cover sediments recognized in the overlying Morcles and Ardon nappes indicates synsedimentary rifting, controlled by the Chamonix normal fault, and the development of the Mont Blanc half graben basin (Boutoux et al. 2014). Compression during the Alpine orogeny compacted the massifs into dome-like structures, but with minor lateral transport and low-grade metamorphism (von Raumer 1969, 1974; Frey et al. 1999; von Raumer and Bussy 2004). The Mont Blanc massif was pressed within a km of the Aiguilles Rouges massif (Fig. 1b), transported a distance of about 20 km or less (von Raumer and Bussy 2004; Boutoux et al. 2014). The southeastern edge of the Mont Blanc massif is bound by the Penninic Front, a major tectonic boundary that separates the Helvetic region (external) of basement massifs and nappes of sedimentary rocks from the high grade metamorphic rocks of the Penninic nappes (internal) (Fig. 1a).

The Vieux Emosson Formation overlies locally highly weathered crystalline basement with more than 0.5 m of local relief (Fig. 2). It consists of up to 10 m of basal conglomerate and sandstone, overlain by up to 10 m of interbedded thin sandstone and shale and thin dolomite beds at the top (Wizevich et al. 2019). Recent analyses of tetrapod trackways revealed the presence of the ichnotaxa *Isochirotherium soergeli* and *Chirotherium barthi* representing a "Chirothere assemblage" of archosaur trackways, thus indicating an Early to Middle Triassic (Late Olenekian to Early Ladinian) age (Avanzini and Cavin 2009; Cavin et al. 2012; Klein et al. 2016). Results of detailed facies analysis along a 20 km belt of outcrop (Fig. 1c) indicate deposition in a shallow braided stream system for the lower unit and in a terminal splay and playa system for the upper unit (Wizevich et al. 2019). Paleocurrent data indicate sediment transport towards the northwest (Fig. 1d), from

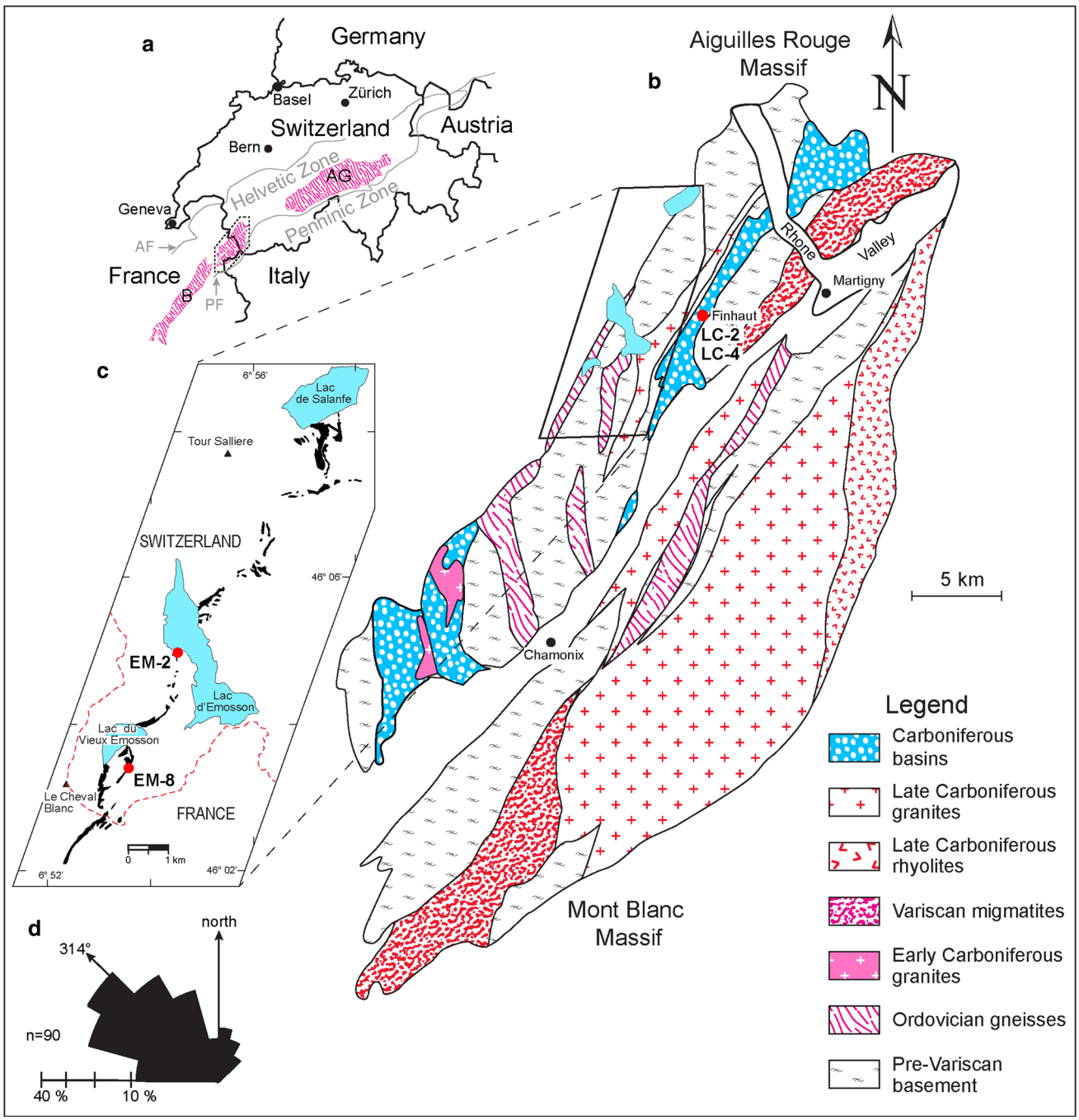

Fig. 1 Location and geologic maps of study area: **a** red patterned areas represent external massifs. *AG* Aar-Gothard massif, *B* Belledonne massif, *AF* Alpine thrust front, *PF* Penninic thrust front; **b** generalized geologic map of the Aiguilles Rouge and Mont Blanc massifs (modified from von Raumer et al. 1999). Also shown are the Late Carboniferous samples, located within the Salvan-Dorénaz basin; **c** outcrop and sample map of Vieux Emosson Formation (black) in the Lake Emosson area (from Collet et al. 1951); **d** Paleocurrent rose diagram (equal area) of trough cross bed indicators taken from bedding plane exposures (e.g., Figure 2a) in the Lake Emosson area

the Vindelician highland toward the Germanic basin (Wizevich et al. 2019). Conglomerates in the lowermost Vieux Emosson Formation contain mostly angular quartz clasts, but locally there are abundant metamorphic lithic fragments (Fig. 2). Sandstones in the lower part of the basal unit are subarkoses, but above a prominent regional internal erosional surface the sandstones are arkoses (Fig. 3).

Sandstone samples were collected from outcrops (Table 1) of the Late Carboniferous Salvan-Dorénaz basin

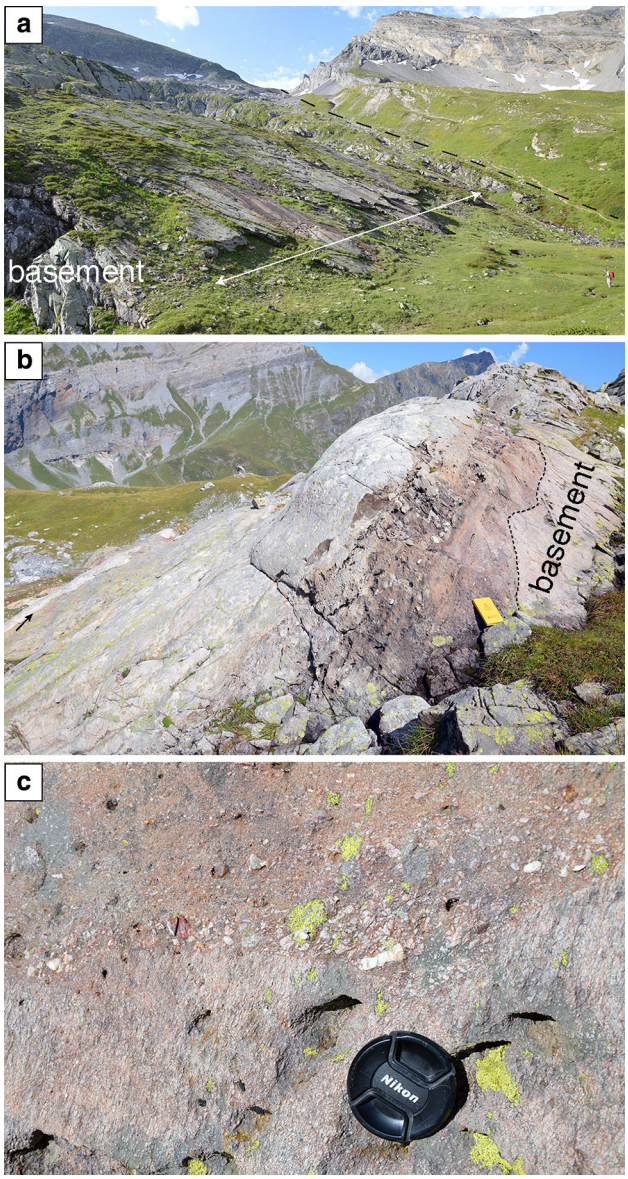

Fig. 2 Outcrop of Vieux Emosson Formation: **a** extensive bedding plane exposure of basal sandstone and conglomerate unit (double arrow), that fining upward to a shale unit. Dashed line indicates contact of formation with overlying allocthonous sedimentary units (Ravin des Ottans locality); **b** basal conglomerate unconformably overlies Aiguilles Rouge basement (Vieux Emosson locality); note internal erosional surface (arrow) separating lighter arkosic sandstones overlying subarkoses (See Fig. 3); and **c** close-up of unconformity in **b**

in Finhaut (LC-2 and LC-4; Fig. 1b) and from the Emosson area (EM-2 and EM-4; Fig. 1c). The stratigraphic positions of the Carboniferous samples are not precisely known, but sample LC-2 is thought to be older. Sample LC-2 was taken from Carboniferous strata and sample LC-4 from Permian strata as marked on the 1:25,000 geologic map (Collet et al. 1951). U–Pb dating of volcanic units in the basin sequence indicates the entire sedimentary fill is of

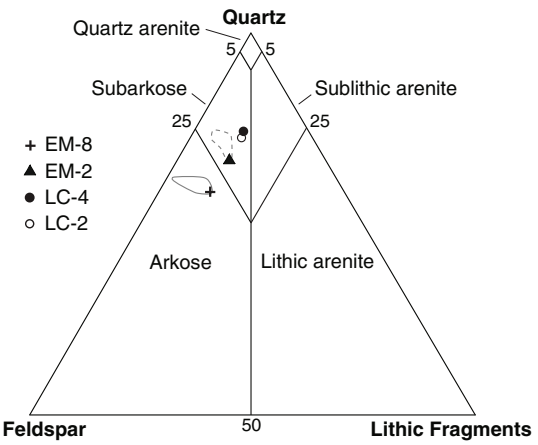

Fig. 3 Compositional diagram of Vieux Emosson Formation and Late Carboniferous sandstones. Other Vieux Emosson Formation samples analysed in Wizevich et al. (2019) are contained within fields. Sandstones below the internal erosion surface (Fig. 2) plot as sub arkoses (n= 5) and those above the surface as arkoses (n= 4)

Late Carboniferous age (Capuzzo and Bussy, 2000). The Triassic samples were taken from the basal sandstone-conglomerate unit of the Vieux Emosson Formation. Sample EM-2 was taken from 2.75 m above the base and sample EM-8 from the top, above the regional internal erosional surface (Fig. 2).

3 Methods

Sandstone composition was determined by petrographic analyses of thin section slides, and consisted of random point counting with a minimum of 300 framework grains and at least 400 total counts. Slides were stained with sodium cobaltinitrite for potassium feldspar.

Zircon concentrates were separated from 2 to 4 kg of sample material at the Senckenberg Naturhistorische Sammlungen Dresden (Museum für Mineralogie und Geologie) using standard methods. Final selection of the zircon grains for U–Pb dating was achieved by hand-picking under a binocular microscope. Zircon grains of all grain sizes and morphological types were selected, mounted in resin blocks, and polished to half their thickness. Concerning stratigraphic ages the stratigraphic time scale of Gradstein et al. (2012) had been used.

Detrital zircon grains of sample EM-2, LC-2, and LC-4 were analysed by a Thermo-Fisher sector field ICP-MS Element 2 XR in combination with a Resonetics Excimer Laser System at the Institute of Geosciences of the Johann Wolfgang Goethe-University Frankfurt (Frankfurt am Main). Zircons from sample EM-8 were analysed for U, Th, and Pb isotopes by LA–SF ICP–MS techniques at the GeoPlasma Lab of the Museum für Mineralogie und Geologie (Dresden), using a Thermo-Scientific Element 2

Table 1 List of detrital zircon samples analysed with corresponding outcrop locations and rock composition

Samples	Locations		Composition
	Swiss grid coordinates (m)	Latitude and longitude	
LC-2	564565	006°58′50″E	Subarkose
	103763	46°05′04″N	
LC-4	564824	006°59′02″E	Subarkose
	103931	46°05′09.5″N	
EM-2	559029	006°54′32.4″E	Subarkose
	103587	46°04′57.2″N	
EM-8	557755	006°53′34.4″E	Arkose
	100562	46°03′19.0″N	

XR sector field ICP–MS coupled to a New Wave UP-193 Excimer Laser System. Each analysis consisted of approximately 15 s background acquisition followed by 30 s data acquisition, using a laser spot-size of 25 and 35 μm, respectively. A common-Pb correction based on the interference- and background-corrected ^{204}Pb signal and a model Pb composition (Stacey and Kramers 1975) was carried out if necessary. Raw data were corrected for background signal, common Pb, laser induced elemental fractionation, instrumental mass discrimination, and time-dependent elemental fractionation of Pb/Th and Pb/U using an Excel® spreadsheet program developed by Axel Gerdes (Institute of Geosciences, Johann Wolfgang Goethe-University Frankfurt, Frankfurt am Main, Germany). Reported uncertainties were propagated by quadratic addition of the external reproducibility obtained from the standard zircon GJ-1 (∼ 0.6% and 0.5–1% for the ^{207}Pb/^{206}Pb and ^{206}Pb/^{238}U, respectively) during individual analytical sessions and the within-run precision of each analysis. Concordia diagrams (2σ error ellipses) and concordia ages (95% confidence level) were produced using Isoplot/Ex 2.49 (Ludwig 2001) and frequency and relative probability plots using AgeDisplay (Sircombe 2004). The ^{207}Pb/^{206}Pb age was taken for interpretation for all zircons > 1.0 Ga. For further details on analytical protocol and data processing see Gerdes and Zeh (2006). Zircons showing a degree of concordance in the range of 90–110% in this paper are classified as concordant because of the overlap of the error ellipse with the concordia. Th/U ratios are obtained from the LA-ICP-MS measurements of investigated zircon grains. U and Pb content and Th/U ratio were calculated relative to the GJ-1 zircon standard and are accurate within approximately 10%. Analytical results of U–Th–Pb isotopes and calculated U–Pb ages are given in Electronic Appendix Table 1.

4 Results

4.1 Description of analysed rocks and minerals

4.1.1 Petrography

The Late Carboniferous samples LC-2 and LC-4 are very poorly sorted metamorphosed sandstones (Fig. 4a, b). Metamorphism is revealed by an apparent alignment (foliation) of fine-grained mica developed in detrital matrix and/or clay cement (nearly 15%), but the sand-size grains are not appreciably affected. The composition of the framework grains indicates the protoliths were subarkosic sandstones (Fig. 3). Quartz grains (∼ 75% of grains) are nearly equal percentages of monocrystalline and polycrystalline varieties. Most feldspar grains have been moderately altered by weathering. Potassium feldspars (∼ 10%) are slightly more abundant than plagioclase (5–8%). Potassium feldspars have been albitized (Fig. 4a, b). Metamorphic rock fragments account for about 10% of the grains. Individual grains are typically subangular. Except for a few small patches of calcite (< 1%), there is no recognizable cement. There is virtually no porosity in either Carboniferous sample.

The Triassic samples EM-2 and EM-8 are subarkosic and arkosic sandstones, respectively (Figs. 3, 4c, d). Both sandstones are poorly sorted and subrounded, although rounding varies from angular to rounded. Sample EM-2 contains twice as much monocrystalline as polycrystalline quartz, whereas in sample EM-8 the ratio is 3–1. Both samples contain about 12% metamorphic rock fragments and K-feldspar is about five times more abundant as plagioclase. Some feldspars show evidence of weathering, but most do not. Both samples contain less than 1% of matrix. Sample EM-2 contains about 20% of fluorite cement and sample EM-8 contains nearly 20% of quartz overgrowth cement. Both samples have less than 1% porosity.

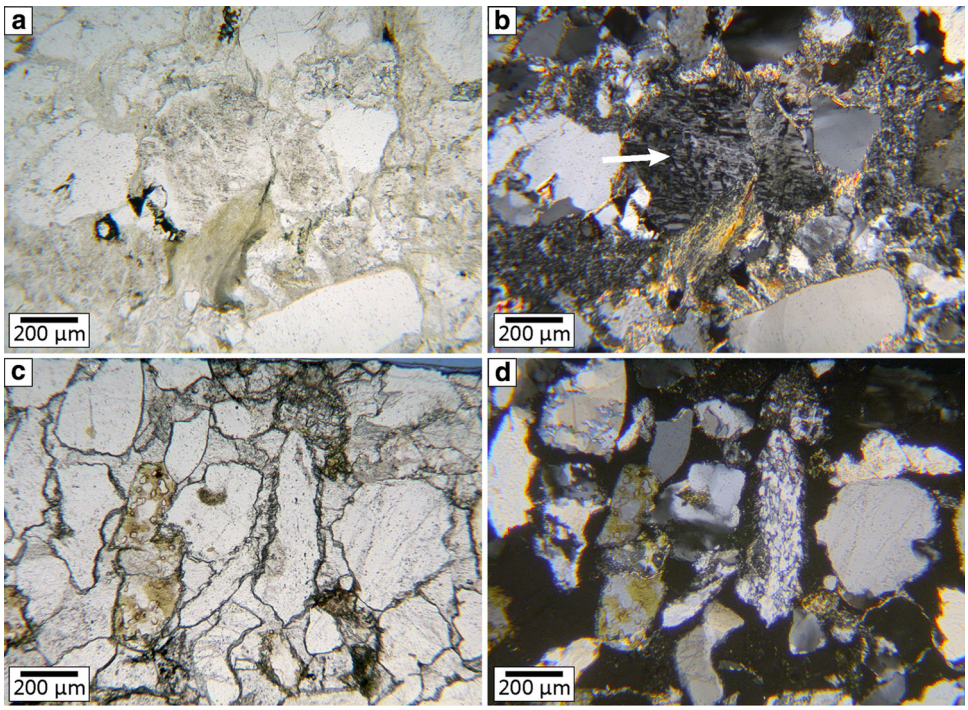

Fig. 4 Photomicrographs of Vieux Emosson Formation and Late Carboniferous sandstones: **a** (plane light) and **b** (crossed nicols) Late Carboniferous sample LC-4. Note illite "whiskers" around grains and albitized potassium feldspar grain (arrow); **c** (plane light) and **d** (crossed nicols) Vieux Emosson sample EM-2. Note abundant potassium feldspar grains with yellow sodium cobaltinitrite stain

4.1.2 Zircons

Nearly all zircons recovered from the four samples are colourless and their grain size varies from 70 to 350 µm, but typically is 120 to 250 µm. Roundness varies for all samples, and most grains that are not broken (~ 50%) exhibit some degree of rounded edges. The Carboniferous samples contain about 35% angular to nearly angular (subangular) grains and less than 10% well rounded grains, whereas the Triassic samples contain about 10% angular to subangular grains and about 30% well rounded grains. For all samples, about half the unbroken zircons are oval ($1.3 <$ length/width < 1.8; Augustsson et al. 2018) and 40–60% are elongated (l/w > 1.8), however the Carboniferous samples contain $< 10\%$ round grains (l/w < 1.3) and the Triassic samples contain 20–25% round grains.

Cathodoluminescence (CL) images of the zircons revealed distinguishing features of zircons, including: internal oscillatory zoning structures, xenocrystic cores, homogeneous luminescence, partial high luminescent cores, and high luminescent rims (Fig. 5). About 30% of the Carboniferous samples and 50% of the Triassic samples showed oscillatory zoning, and all samples typically had 10–15% zircons with xenocrystic cores. For all samples between 25 and 35% of the zircon grains were homogenous in CL and about 10–15% showed partial high luminescent cores. About 45% of the Carboniferous samples and 25% of the Triassic samples contained high luminescent rims that are typically only a few µm thick, but rarely the rims may be up to a few tens of µm thick (Fig. 5d).

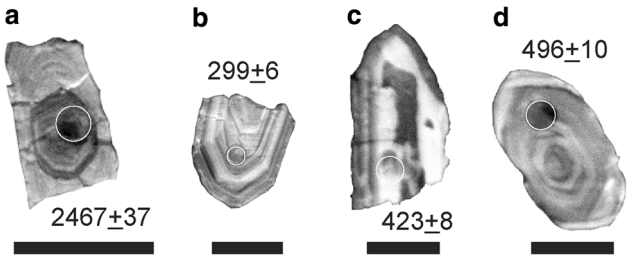

Fig. 5 Cathodoluminescence (CL) images of representative zircon samples. Analysed spots are outlined in white. Resultant $^{206}Pb/^{238}U$ apparent ages (in Ma) are shown with 2σ errors. Scale bars are 100 µm: **a** Distinct xenocrystic core within zircon with oscillatory zoning (sample EM-2); **b** Zircon with oscillatory zoning (sample EM-2). **c** Zircon with patchy internal high luminescence (sample LC-4); **d** Zircon with oscillatory zoning and a high luminescent rim (sample EM-8)

4.2 Zircon U–Pb ages

Table 1 of the Electronic Appendix presents the results of the U–Pb analyses, and Fig. 6a–d contains the concordia curves of all zircons analysed. Probability density plots in Figs. 6 e–h and 7 show only results of analyses with calculated U–Pb ages within 10% of concordance. Table 2 contains a summary of the ages of significant peaks in the detrital zircon age distribution plots (Figs. 6, 7).

4.2.1 Sandstones from the Salvan-Dorénaz basin

The probability curves for the Late Carboniferous samples LC-2 and LC-4 (Figs. 6g, h, 7) show multiple peaks

throughout the Neoproterozoic to Palaeozoic ages. Only 17 zircons were within the 10% error margin for sample LC-2, but they provide similar age spectra like sample LC-4 with few exceptions. Sample LC-4 has detrital age patterns dominated by Cambrian-Ordovician (444, 466, 482 and 506 Ma) and late Neoproterozoic (542, 603 635 and 664 Ma) age peaks with smaller Carboniferous (319 Ma), Late and Middle Devonian (368 and 395 Ma) and earlier Neoproterozoic (e.g., 753, 783 and 961 Ma) peaks (Fig. 7). One Paleoproterozoic zircon (2.43 Ga) was found in sample LC-4. The probability curves for sample LC-2 indicate most of the zircons to have Early Carboniferous (323, 336 and 349 Ma) and Late and Middle Devonian (367 and 395 Ma) ages and small peaks in late Cambrian (502) and Neoproterozoic (601 and 836 Ma). One Mesoproterozoic zircon (1.60 Ga) was found in sample LC-2.

4.2.2 Vieux Emosson Formation

The probability curves for the Triassic sandstones samples EM-2 and EM-8 (Figs. 6e, f and 7) also show numerous peaks, but have subtle differences with the Late Carboniferous samples and between themselves. The curve for sample EM-2 contains primary peaks in the Late Carboniferous (299 and 314 Ma) and Permian (251, 263, 270, and 285 Ma), Early Devonian (408 Ma) Silurian (430 and 441 Ma), lesser peaks in the Late and Middle Devonian (359 and 380 Ma), Middle Ordovician (469 Ma), Cambrian (506 and 526 Ma) and latest Neoproterozoic (553 Ma), and several smaller peaks in the earlier Neoproterozoic (e.g., 708, 771, 931 and 992 Ma). Two Mesoproterozoic (1.49 and 1.56 Ga) and seven Paleoproterozoic (1.69, 1.74, 1.93, 2.02, 2.13, 2.28 and 2.47 Ga) zircons were identified in sample EM-2. The probability curves for sample EM-8 contain two major peaks in the late Cambrian (494 Ma) and Early Ordovician (471 Ma), with smaller peaks in the middle Carboniferous (323 Ma), Late Devonian (374) and Neoproterozoic (558, 691 and 800 Ma). One Mesoproterozoic (1.68 Ga) and three Archean (2.58, 3.02 and 3.47 Ga) zircons were identified in sample EM-8.

5 Discussion

Features like high luminescent cores and rims represent metamorphic recrystallization and replacement of zircons (Corfu et al. 2003). Although most rims are too small for dating, the relatively high percentage of Carboniferous samples with rims compared to the Triassic samples suggests that many of the rims originated from metamorphic growth during the Variscan overprint.

Arkosic and subarkosic composition and immature textural attributes of the Triassic sandstones and conglomerates in the Vieux Emosson Formation suggest short transport and derivation largely from local Aiguilles Rouges basement sources (Fig. 1b). Northwest paleocurrents suggest the streams were fed from drainage basins located to the southeast. The Mont Blanc massif was also a likely source because of the near proximity ($\sim$ 20 km before being shortened by Alpine folding). Both massifs shared a similar geologic evolution and consist of similar metamorphic and igneous rocks (von Raumer et al. 1999; von Raumer and Bussy 2004) (Fig. 1b; Table 3).

5.1 Detrital zircons and basement age dates

The wide range of detrital zircon age dates from the Carboniferous and Triassic sandstones (Figs. 6 and 7; Table 2) reflect the complex basement that comprises the massifs. The Aiguilles Rouges basement includes a diverse assemblage of polymetamorphosed lithologies, comprising orthogneiss, amphibolites, eclogites, serpentinite, paragneiss, mica schist, marble, and quartzite (von Raumer and Bussy 2004); and its origin, as well as that of the other Alpine basement areas, is attributed to a typical Cadomian evolution on the Gondwanan margin (von Raumer and Stampfli 2008; von Raumer et al. 2013). Most of the polymetamorphic basement is composed of gneisses and mica schists that have a sedimentary origin (von Raumer and Bussy 2004), and thus may not be directly dated. However, because inherited and detrital zircon geochronology has generated a reasonably good understanding of the pre-Variscan basement evolution, we may compare the main age groups of the age-date probability curves (Figs. 6 and 7) with already published results. Table 3 comprises published radiometric age data from Aiguilles Rouges and Mont Blanc massifs and von Raumer et al. (2013, fig. 3 and references therein) provide information about existing age data for the Alpine basement areas. Summarizing the results, three main periods of ages may be differentiated: Neoproterozoic-Cadomian, Cambro-Ordovician, and Carboniferous-Permian Variscan and post-Variscan periods. In addition, two other time periods are represented by detrital zircons in this study, pre-Cadomian, Silurian-Devonian (Table 2) and will be discussed as well.

5.1.1 Neoproterozoic-Cadomian and Pre-Cadomian periods

The complex geotectonic evolution of the external massifs began in the mid-Neoproterozoic, when the Cadomian Orogen developed in an active margin setting along the northern edge of Gondwana (Linnemann et al. 2007). The orogeny represents a Cordilleran-type orogen and consisted of several pulses of magmatism from $\sim$ 750 Ma until

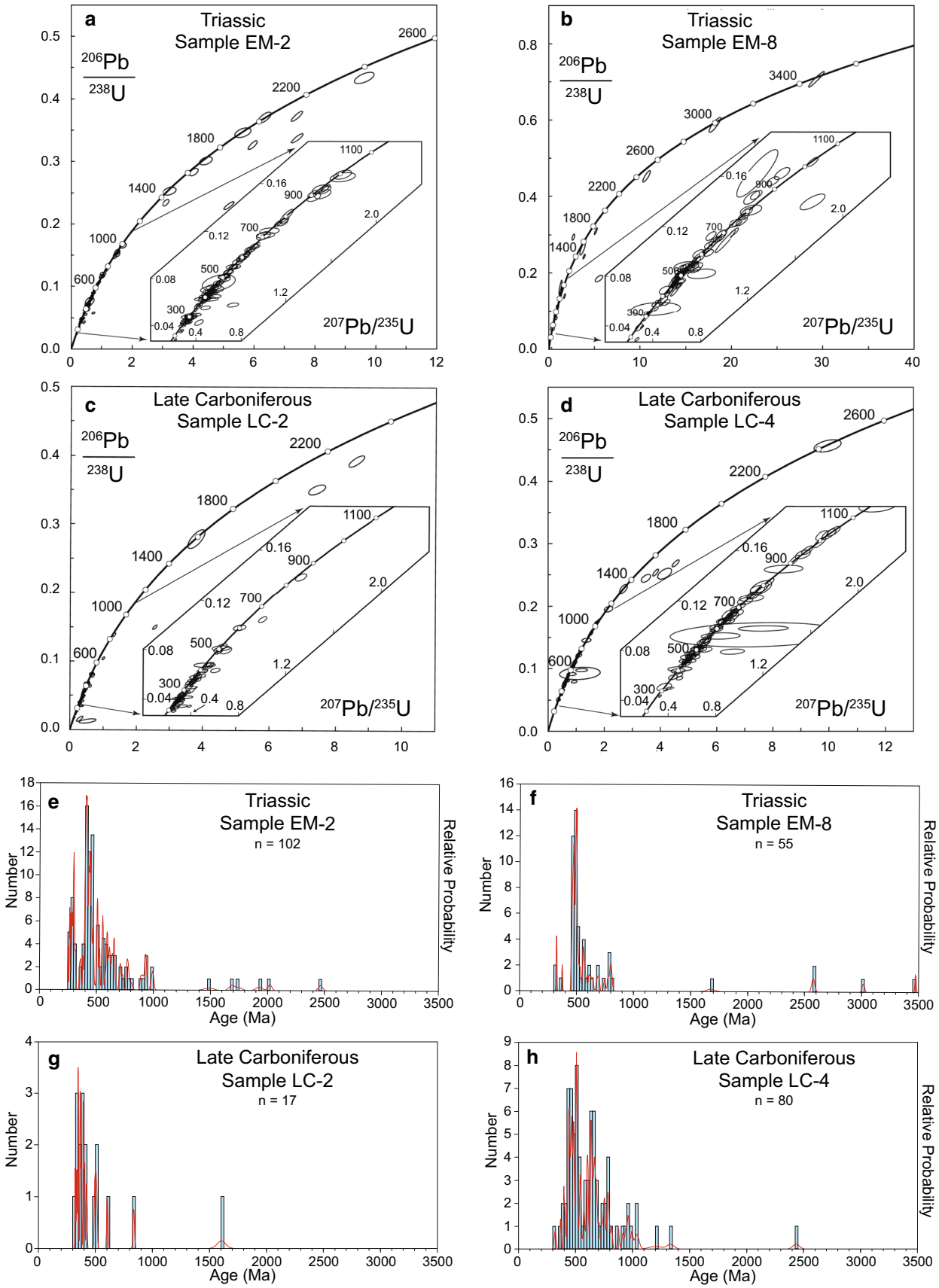
a
Triassic
Sample EM-2
b
Triassic
Sample EM-8
c
Late Carboniferous
Sample LC-2
d
Late Carboniferous
Sample LC-4
206Pb/238U
207Pb/235U
e
Triassic
Sample EM-2
n = 102
f
Triassic
Sample EM-8
n = 55
g
Late Carboniferous
Sample LC-2
n = 17
h
Late Carboniferous
Sample LC-4
n = 80
Number
Relative Probability
Age (Ma)

◀**Fig. 6** U–Pb ages of detrital zircon grains from Triassic samples (EM) and Late Carboniferous (LC) samples. **a–d** Concordia curves with detailed views of 250 to 1100 Ma shown in insets for each sample. Data-point error ellipses are 2σ. **e–h** Combined binned frequency and probability density plots for results of all zircon age analyses with ages with discordance > 10% omitted. Bin width is 25 Ma

early Cambrian grantoid plutonism marked the end of the Cadomian Orogeny (Linneman et al. 2008, 2014).

Zircons with age dates ~ 650–550 Ma are common in peri-Gondwana derived terranes (Gebauer 1993; Schaltegger 1993, 1994; Schaltegger and Gebauer 1999; Gerdes and Zeh 2006). Similar age dates (650–570 Ma) of detrital zircons are common in metasediments from the external massifs of the Central Alps (Aar and Gothard massifs, Fig. 1a) (e.g., Gebauer 1993; Schaltegger and Gebauer 1999). Detrital zircons with late Neoproterozoic ages are abundant in the Carboniferous sandstones, but are also, at a lesser degree, found in the Triassic sandstones, thus confirming sources of detritus of Cadomian basement in this Alpine domain (Fig. 7).

Detrital zircons with age dates that are older than Cadomian magmatism represent recycled detrital zircons were likely deposited in Neoproterozoic-Cambrian peri-Gondwanan basins (von Raumer et al. 2002; Linnemann et al. 2007; Garfunkel 2015). Older Neoproterozoic detrital zircons (~ 700–800 Ma), prominent in the Vieux Emosson Formation and LC-2 samples, are not recognized in the Helvetic basement domain (see compilation charts in Linnemann et al. 2008; von Raumer et al. 2013; and Beltrán-Triviño et al. 2013). These dates and those of the earliest Neoproterozoic (~ 900–1000 Ma) reflect an East-African-Arabian zircon province source area for the metasedimentary zircons (Meinhold et al. 2013; Siegesmund et al. 2018; Stephan et al. 2019a; Couzinié et al. 2019). Older zircons were probably derived from East-African–Arabian (1.1–1.5 Ga, 1.65–1.85 Ga, 2.45–2.7 and 2.6–3.1 Ga) and West African cratons (1.8–2.2 Ga and 3.1–3.4 Ga) (Linnemann et al. 2007 and references therein). The oldest dated zircon of 3.47 Ga (sample EM-2) is slightly older than the 3.43 Ga date from Gebauer (1993), the previously oldest dated zircon in Alpine basement, and likely came from the 3.4–3.5 Ga terrane in the West African craton (Potrel et al. 1996).

Although the abundant detrital zircons with late Neoproterozoic ages in the Carboniferous and Triassic samples support a Cadomian origin for the basement source, the older detrital zircons are not useful for further pinpointing the paleogeographic position within the peri-Gondwana domain. For instance, some of the oldest zircons may be sourced from remnants of older (pre-Neoproterozoic)

Table 2 Relative amounts (X = few to XXX = many) of detrital zircons with age dates for specific time periods for Triassic and Late Carboniferous samples

	Variscan & Post-Variscan				Cambro-Ordovician	Cadomian & Earlier (Recycled)			
						Proterozoic			
	Permian 250-300 Ma	Carboniferous		Devonian-Silurian 350-450 Ma	Ordovician-Cambrian 450-550 Ma	Neo- 550-650 Ma (l) 650-800 Ma(m) 875-1000Ma (e)	Meso- 1.0-1.6 Ga	Paleo- 1.6-1.8 Ga (l) 1.8-2.2 Ga (m) 2.2-2.6 Ga (e)	Archean 2.5-3.5 Ga
		Late 300-325 Ma	Early 325-350 Ma						
Triassic Vieux Emosson Formation									
EM-8		XX			XXX	XX(l)		X(e,m,l)	X
EM-2	XX	XX		XXX	XX	XX(l) & X(e)	X	X(l)	
Late Carboniferous Metasedimentary Basement									
LC-4		X		XXX	XXX	X (l & e)	X	X(e)	
LC-2		X	XX	XXX	XX	XX (l, m & e)		X(l)	

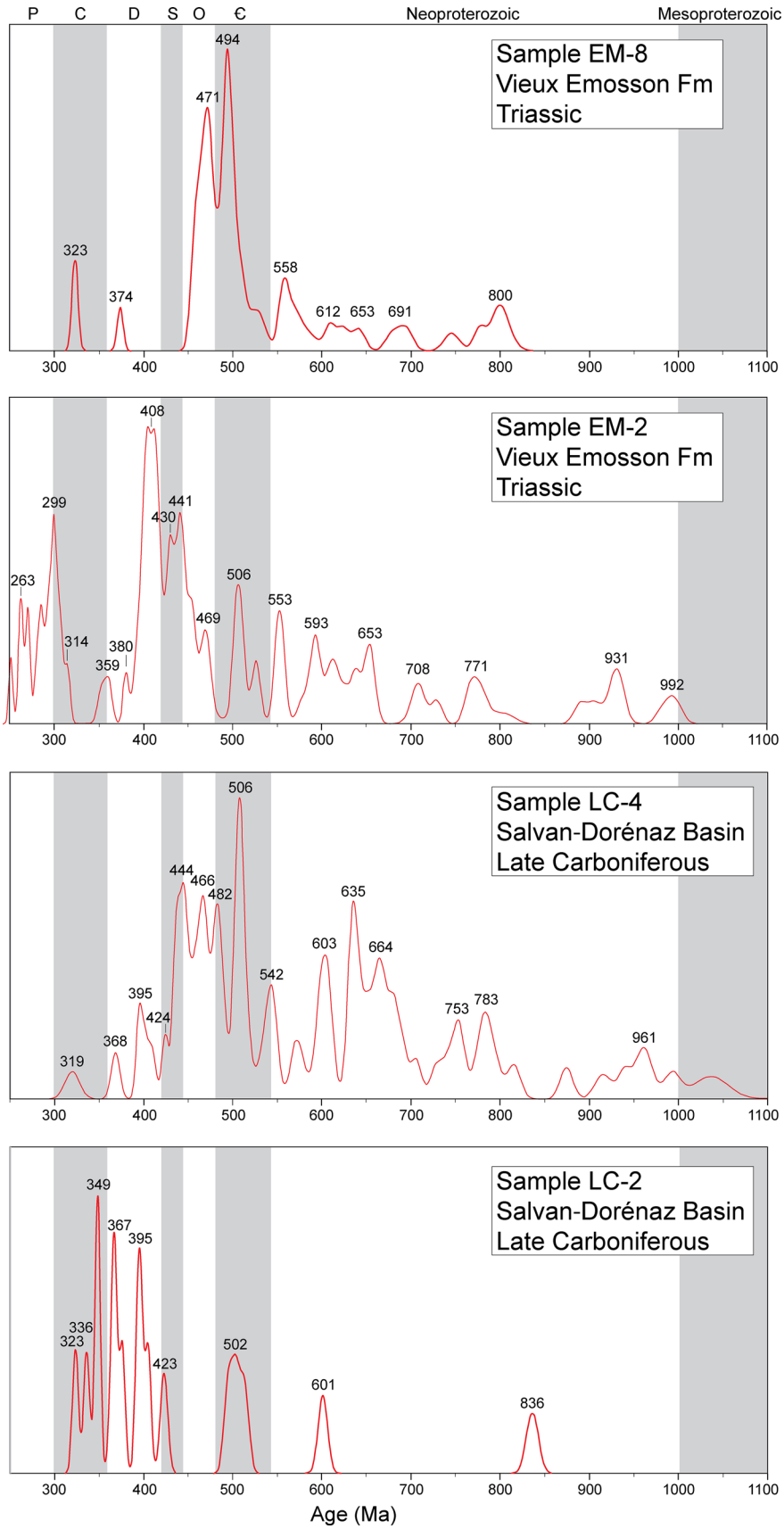

Fig. 7 Detailed views of probability curves between 250 and 1100 Ma with Paleozoic periods and Neoproterozoic and Mesopaleozoic eras delineated

Table 3 Compilation of isotopic age dates of rock units in the Aiguilles Rouges and Mont Blanc massifs

Zircon bearing unit*	Zircon age (Ma)	References
Igneous units		
Aiguilles Rouges massif		
Salvan-Dorenzaz basin		Capuzzo and Bussy (2000)
Tuffs	295 +3/-4	
Dorénaz dacite volcanic	308 ± 3	
Rhyolitic dike	311 ± 17	
Morcles microgranite	303 ± 2	Grosjean et al. (2018)
	309–312	
Vallorcine granite	306.5 ± 1.5	Bussy et al. (2000)
Fully gabbros	307 ± 2	
Porménaz granite	332 ± 2	
Montées Pélissiers granite	331 ± 2	
Mont Blanc massif		
Mont Blanc granite	303 ± 2	Bussy et al. (2000)
Montenvers granite	307 ± 3	
Mont Blanc rhyolite	307 ± 2	Capuzzo and Bussy (2000)
Lognan granite	453 ± 3	Bussy and von Raumer (1994)
Polymetamorphic basement		
Aiguilles Rouges massif		
Emosson leucosome	320 ± 1*	Bussy et al. (2000)
Emosson micaschists	327 ± 2*	
Garnet gneisses	~300–330*	Schulz and von Raumer (2011)
Mylonitic garnet gneisses	~440*	
Eclogite	453 +3/− 2	Paquette et al. (1989)
Lake Cornu augengneiss	455 +3/− 4	Bussy et al. (2011)
Mt Lusin orthogneiss	455.3 ± 0.6	
Eclogitic amphibolite	458 ± 5	
Val Bérard orthogneiss	461 +3.5/− 4.5	
Banded eclogite	463 +3/− 2	
Val Bérard augengneiss	464 +5/− 3	

All dates are from zircons except for metamorphic dates (*) which are from monazite

crustal material that may have been incorporated into the Cadomian domain (Linneman et al. 2008; Abbo et al. 2015; Garfunkel 2015; Avigad et al. 2018). However, it should be noted that although crustal fragments of pre-Neoproterozoic basement have been identified within Cadomian-type terranes throughout Europe, they have not yet been reported in the Alpine regions (see Garfunkel, 2015, fig. 4a). It is also possible that long-distance river transport, possibly in multiple recycling stages, may have supplied the Grenville (~ 1 Ga) and pre-Neoproterozoic detrital zircons from the far margins of Gondwana to the Cadomian basins (e.g., Meinhold, et al. 2013; Stampfli et al. 2013; Rösel et al. 2014).

5.1.2 Cambro-Ordovician periods

The northern Gondwana margin underwent major plate-tectonic transition from compressional to extensional tectonics during middle to late Cambrian with the rifting of Avalonia from Gondwana and the Early Ordovician opening of the Rheic Ocean (Linnemann et al. 2007; Nance et al. 2010, 2012). The Chamrousse meta-ophiolite sequence (496 Ma) in the Belledonne massif (Fig. 1a) may represent the Cambrian episode of rifting and seafloor spreading (Ménot et al. 1988), and counterparts of it may be the ultramafic lenses observed near the Lac Comu area (Aiguilles Rouges) (von Raumer and Bussy 2004). A mafic metavolcanic in the western end of Aiguilles Rouges is geochemically different and, although not dated, is thought to be of Ordovician age (Dobmeier et al. 1999).

In the Alpine Cadomian terranes, including the external massifs, after (back-arc?) rifting developed in the Cambrian–Ordovician, the terranes were subsequently re-accreted to the Gondwana margin during a short-lived Cordilleran-type orogen (Stampfli et al. 2002; Schaltegger et al. 2003; Bussy et al. 2011; von Raumer et al. 2013).

Magmatism developed during the aborted rifting during the late Cambrian-Early Ordovician, coeval with the separation of Avalonia from Gondwana and the opening of the Rheic Ocean, and subsequent (mid-Ordovician) re-accretion of the terrane (Stampfli et al. 2002; von Raumer et al. 2013). In the external massifs, Ordovician (~ 480–450 Ma) arc volcanism is recognized by orthogneisses, which are interpreted as granitoids that intruded into sedimentary units (now paragneiss) (von Raumer et al. 2002, 2013; von Raumer and Bussy 2004; Bussy et al. 2011; Table 3).

In this study, all samples contained abundant late Cambrian (~ 500 Ma) zircons, which can be correlated to the Cambrian rifting events (von Raumer and Stampfli 2008; von Raumer et al. 2013). The subsequent Ordovician magmatic evolution is not only well documented in the study area (Table 3), but is also well documented through its detrital zircons (Fig. 7).

5.1.3 Silurian-Devonian, Carboniferous-Permian Variscan and post-Variscan periods

Numerous, often disparate, geodynamic models that have been proposed for the Late Palaeozoic Variscan orogeny, which arose from the collision of the Cadomian terranes and Gondwana with Laurussia. For example, there are conflicting models as to whether the terranes separated during the Silurian-Early Devonian from Gondwana as an assemblage of microplates separated by intervening ocean crust (e.g., Franke 2000; Matte 2001; Stampfli et al. 2002; von Raumer et al. 2013; Franke et al. 2017) or remained attached to Gondwana on stretched continental crust as a contiguous shelf south of the Rheic Ocean (i.e., "one ocean model") until the orogeny (Robardet 2003; Kroner and Romer 2013; Žák and Sláma 2018; Romer and Kroner 2019; Stephan et al. 2019a, b). In the microplates model, Late Ordovician and Silurian extension of the Cadomian crust preceded the opening of the Paleotethys oceanic domain (von Raumer and Stampfli 2008; Stampfli et al. 2011; von Raumer et al. 2013). An important difference between the two models is that with the one ocean model Cadomian terrane would be tectonically quiescent during the Silurian-Early Devonian, but in the splintered terranes model, there would be rifting and ocean crust development as well as volcanic arc tectonism during that interval.

Detrital zircons of Silurian and Early Devonian ages are abundant in samples LC-4 and EM-2. Middle Paleozoic metamorphic or magmatic events are not recognized in the External Massif basement, but are identified in the other Alpine terranes (see Beltrán-Triviño et al. 2013, fig. 2 and von Raumer et al. 2013, fig. 3). This finding may indicate unidentified, completely eroded or distal (non-massif) source areas with Silurian and Early Devonian zircons and supports the multiple ocean models. Alternatively, magmatism related to the Silurian amalgamation of Baltica-Avalonia-Laurentia (e.g., Anthes and Reischmann 2001), which formed Laurussia and lies to the north of the study area, may be a potential source for Silurian zircons. Considering the northwestern oriented paleocurrents (Wizevich et al. 2019), it is unlikely that the Triassic rivers drained from an Avalonia source area. Nevertheless, it is possible that zircons were transported from the north during Late Carboniferous sedimentation in the Salvan-Dorénaz basin and were subsequently reworked into the Triassic sediments. Paleocurrent data from the Late Carboniferous metasedimentary units indicate sediment transport from the SW and NE (Capuzzo and Wetzel, 2004). Similarly, ample amounts of Silurian and Early Devonian detrital zircons were found in the Mels Formation, autochthonous Triassic of the Aar massif, although no potential source rock is known to exist in the massif (Fig. 1, Beltrán-Triviño et al. 2013). The source of the zircons may have been generated by late stages of magmatic activity related to the Ordovician orogenic event (Beltrán-Triviño et al. 2013), however, there are Carboniferous basins within the Aar massif (Schaltegger and Corfu 1995) and thus recycling of Avalonian zircons may also be possible.

Collision of the Cadomian terranes with the European (Laurussia) continent, initiating the Variscan orogeny, began around Middle Devonian time (~ 380 Ma) and was followed by continued compression, large-scale strike-slip movement and jumbling of the terranes against Laurussia, and widespread high-temperature overprint with granitic intrusions and migmatitization in Late Carboniferous (~ 320–305 Ma) time (von Raumer et al. 2009, 2013). Post-Variscan magmatism (~ 305–295 Ma) was generated by underplating of mantle-derived magmas, caused by crustal extension of an unresolved nature (for review of potential causes of extension see discussion in Grosjean et al. 2018).

The Upper Devonian (380–359 Ma) and Carboniferous-Permian (349–263 Ma) detrital zircons (Fig. 7; Table 2) can be correlated with the Variscan orogeny and post-Variscan igneous rocks. Early Variscan zircons (e.g., 380, 358 and 349 Ma) are not represented in the basement, but are equally abundant as zircons derived from the Late Carboniferous-Early Permian basement (Fig. 6; Table 3). Similar early Variscan ages are also reported for the Mels Formation (Beltrán-Triviño et al. 2013), but potential source rocks have not been reported for the Aar massif (Ballèvre et al. 2018). Late Carboniferous age zircons in the samples LC-2 and LC-4 supports rapid exhumation of the basement as proposed by Capuzzo and Wetzel (2004).

Sample EM-2 contains several Permian-age detrital zircons presenting an interesting conundrum. Permian age-dates are rare in the external massifs, but are prevalent in the Alpine basement east of Mont Blanc (e.g., Bertrand

et al. 2000; Beltrando et al. 2007; Bergomi et al. 2017; Ballèvre et al. 2018; Kunz et al. 2018 and references therein). Permian low-pressure-high-temperature metamorphism and igneous activity associated with post-orogenic lithospheric thinning of the Variscian has been recognized in the Penninic and Austroalpine Alps with zircon age dating (Schuster and Stüwe 2008). Permian age (~ 270 Ma) zircons found in Late Carboniferous microgranitic dykes of the Aiguilles Rouges massif may be attributed to fluid circulation related to the emplacement of U-rich brecciated veinlets of ~ 256 Ma (Meisser 2012) located close to the Salvan-Dorénaz basin (Grosjean et al. 2018). It is possible that zircons altered by fluid circulation may have been incorporated into the sediments, but the wide spread of Permian ages in sample EM-2 suggests other sources may be likely as well.

5.2 Provenance analysis

Overall, the detrital zircon ages dates from both the Triassic and Late Carboniferous samples indicate derivation largely from local basement, but with the primary components somewhat different for each sample (Fig. 6; Table 2). Numerous Cadomian and Cadomian recycled (pre-Late Neoproterozoic), Odovician, Carboniferous, and probably late Cambrian zircons (Figs. 6 and 7) can be directly associated with Helvetic basement domains (Table 3; von Raumer et al. 2013). Silurian, Devonian, Early Carboniferous, and Permian zircons, however, cannot be directly correlated to the local basement.

Except for abundant early Variscan (Devonian) and Permian ages from sample EM-2, age distributions from it and sample LC-4 are very similar (Fig. 7; Table 2), suggesting similar source areas for the two samples and/or significant reworking of the Carboniferous sediments into the Triassic unit. The albitized feldspar found only in the Carboniferous samples suggests minimal, if any, recycling. Feldspar albitization is typically a burial process, however it may also form from sodium-rich fluid percolating through rock or sediments and has been recognized on post-Hercynian paleosurfaces in the Massif Central of France (Simon-Coinçon 1999). Either way, locally derived albitized feldspars from the Carboniferous sandstones should have survived the short transport and would be recognized in the Vieux Emosson Formation samples. The differences in zircon morphology between the Carboniferous and Triassic samples may correspondingly reflect different source areas, but it may also reflect sorting as a result of different depositional processes (Augustsson et al. 2018). The Carboniferous sandstones were also deposited in fluvial systems, but paleocurrent indicators reveal a wide range of transport directions, primarily from the northwest, southwest, east and northeast (Capuzzo and Wetzel 2004).

The younger Triassic sample (EM-8) differs from the other samples with no Silurian, Early Devonian or Early Neoproterozoic (~ 900–1000 Ma) zircons (Fig. 6; Table 2). Sample EM-8 also differs from sample EM-2 by containing abundant Ordovician zircons. These differences indicate a significant change in the source area in the uppermost sandstone units, reflecting a more local source area primarily composed of Ordovician orthogneiss. This interpretation is supported by the more feldspathic composition of sample EM-8 (Fig. 3).

Possible explanations for the absence of local source rocks for the Silurian-Devonian and Permian, and to a lesser extent, late Cambrian zircons are that either the source rocks zircons are not yet recognized, they were eroded away, or they were hidden by Alpine tectonism. Source areas farther to the southeast are also possible, but Alpine deformation and metamorphism have obfuscated the exact nature of the region at the time of the deposition of the Vieux Emosson Formation. It is beyond the scope of this paper to speculate on the position of the terranes to the southeast of the external massifs during Early-Middle Triassic time. Reconstructions of this area based on geophysical data indicate that the Penninic nappes are thrust upon basement that extends from the external massifs (Schmid et al. 1996; Stampfli et al. 2002). The nature of the basement beneath the Penninic nappes is not known. Since some of the source rocks, likely beneath the nappes, have elements of Penninic and Austroalpine domains, it appears that these domains may have a closer affinity with the Helvetic basement domain as thought by some (e.g., Froitzheim 2001; Beltrando et al. 2007) and not by others (e.g., Ring et al. 2005).

6 Conclusions

The age data of the detrital zircons in the Triassic Vieux Emosson Formation and in the sandstones from the Late Carboniferous Salvan-Dorénaz basin indirectly confirm the presence of Cadomian basement in the external massifs of the Western Alps. Early Cambrian and late Neoproterozoic (~ 520–750 Ma) zircons are commonly found in Alpine basement and are correlated to the Cadomian origin of this basement. Pre-late Neoproterozoic zircons found in all samples were likely derived from metasedimentary (paragneiss) units, which were deposited in basins within the Cadomian terrane. Some of these older zircons may have been reincorporated (and preserved as cores) into younger igneous rocks during later magmatic events (e.g., Ordovician and Carboniferous) that intruded the sediments. The older recycled zircons, including a 3.47 Ga zircon that represents the oldest Alpine detrital zircon, are likely originally from source areas in the East-African–Arabian

and West African cratons. Abundant Ordovician-age zircons were derived from the orthogneiss of the massifs (Fig. 1). The relative paucity of Carboniferous ages suggests that the granites presently exposed on the massifs (Fig. 1) were not widely exposed at the surface during the time of sedimentation. Overall, the Carboniferous metasedimentary rocks and the Triassic sandstones were both largely derived from local basement. There appears to be little, if any, recycling of the Carboniferous sediments into the Vieux Emosson Formation. The two Vieux Emosson samples, separated by a marked erosional surface in the Triassic strata, have distinctly different sandstone and detrital zircon compositions, which suggests somewhat different source areas.

A significant number of Silurian, Devonian, Early Carboniferous, Permian, and to a lesser degree, late Cambrian detrital zircons in the Vieux Emosson Formation represent rocks that have not been widely recognized in the external massifs, but are relatively abundant in the Penninic and Austroalpine domains. Possible source areas include local basement rock types that have been entirely eroded away, or hidden basement that extends from the Helvetic domain beneath the Penninic nappes, or both. The late Cambrian, Silurian, and Permian detrital zircons in the source area suggests more similarities with the Helvetic basement and the Penninic and Austroalpine domains than previously recognized.

Acknowledgements We thank Basil Thüring, Sylvan Thüring, Henrik Klein, Petra Eggenschwiler, Sylvia Schmutz, and Justin Ahern for assistance in the field. Andreas Wetzel provided MW support at the University of Basel during summer visits. Funding for MW was provided by Connecticut State Universities–AAUP research grants. The Natural History Museum Basel provided financial support for field work with its "Fonds für Lehre & Forschung". Armin Zeh is thanked for his help with the U–Pb LA-ICP-MS zircon dating at the Institute of Geowissenschaften at the Goethe University of Frankfurt am Main. Finally, we thank J.F. von Raumer and D. Bussien Grosjean for their constructive reviews as well as Editor W. Winkler, for his helpful handling of the manuscript.

References

Abbo, A., Avigad, D., Gerdes, A., & Güngör, T. (2015). Cadomian basement and Paleozoic to Triassic siliciclastics of the Taurides (Karacahisar dome, south-central Turkey): paleogeographic constraints from U–Pb–Hf in zircons. *Lithos, 227,* 122–139.

Anthes, G., & Reischmann, T. (2001). Timing of granitoid magmatism in the eastern mid-German crystalline rise. *Journal of Geodynamics, 31,* 119–143.

Augustsson, C., Voigt, T., Bernhart, K., Kreißler, M., Gaupp, R., Gärtner, A., Hofmann, M., & Linnemann, U. (2018). Zircon size-age sorting and source-area effect: The German Triassic Buntsandstein Group. *Sedimentary Geology, 375,* 218–231.

Avanzini, M., & Cavin, L. (2009). A new isochirotherium trackway from the Triassic of Vieux Emosson, SW Switzerland: Stratigraphic implications. *Swiss Journal of Geosciences, 102,* 353–370.

Avigad, D., Rossi, P., Gerdes, A., & Abbo, A. (2018). Cadomian metasediments and Ordovician sandstone from Corsica: Detrital zircon U–Pb–Hf constrains on their provenance and paleogeography. *International Journal of Earth Sciences, 107,* 2803–2818.

Ballèvre, M., Manzotti, P., & Dal Piaz, G. V. (2018). Pre-Alpine (Variscan) inheritance: A key for the location of the future Valaisan Basin (Western Alps). *Tectonics, 37,* 786–817.

Beltrando, M., Rubatto, D., Compagnoni, R., & Lister, G. (2007). Was the Valaisan basin floored by oceanic crust? Evidence of Permian magmatism in the Versoyen Unit (Valaisan domain, NW Alps). *Ofioliti, 32,* 85–99.

Beltrán-Triviño, A., Winkler, W., & Quadt, A. (2013). Tracing Alpine sediment sources through laser ablation U–Pb dating and Hf-isotopes of detrital zircons. *Sedimentology, 60,* 197–224.

Bergomi, M. A., Dal Piaz, G. V., Malusà, M. G., Monopoli, B., & Tunesi, A. (2017). The grand St Bernard-Briançonnais Nappe system and the Paleozoic inheritance of the Western Alps Unraveled by Zircon U–Pb dating. *Tectonics, 36,* 2950–2972.

Bertrand, J. M., Pidgeon, R. T., Leterrier, J., Guillot, F., Gasquet, D., & Gattiglio, M. (2000). SHRIMP and IDTIMS U–Pb zircon ages of the pre-Alpine basement in the Internal Western Alps (Savoy and Piemont). *Schweizerische Mineralogische und Petrographische Mitteilungen, 80,* 225–248.

Boutoux, A., Bellahsen, N., Lacombe, O., Verlaguet, A., & Mouthereau, F. (2014). Inversion of pre-orogenic extensional basins in the external Western Alps: Structure, microstructures and restoration. *Journal of Structural Geology, 60,* 13–29.

Bussy, F., Hernandez, J., & von Raumer, J. (2000). Bimodal magmatism as a consequence of the post-collisional readjustment of the thickened Variscan continental lithosphere (Aiguilles Rouges-Mont Blanc Massifs, Western Alps). *Earth and Environmental Science Transactions of The Royal Society of Edinburgh, 91,* 221–233.

Bussy, F., Péronnet, V., Ulianov, A., Epard, J. L., von Raumer, J., Gutiérrez-Marco, J. C., Rábano, I., & García-Bellido, D. (2011). Ordovician magmatism in the external French Alps: Witness of a peri-Gondwanan active continental margin. In J. C. Gutiérrez-Marco, I. Rabano, & D. García-Bellido (Eds.), *Ordovician of the World* (pp. 75–82). Madrid: Instituto Geológico y Minero de España.

Bussy, F., & von Raumer, J. (1994). U–Pb geochronology of Palaeozoic magmatic events in the Mont-Blanc Crystalline Massif, Western Alps. *Schweizerische Mineralogische und Petrographische Mitteilungen, 74,* 514–515.

Capuzzo, N., & Bussy, F. (2000). High-precision dating and origin of synsedimentary volcanism in the Late Carboniferous Salvan-Dorénaz basin (Aiguilles-Rouges Massif, Western Alps). *Schweizerische Mineralogische und Petrographische Mitteilungen, 80,* 147–167.

Capuzzo, N., Handler, R., Neubauer, F., & Wetzel, A. (2003). Post-collisional rapid exhumation and erosion during continental sedimentation: the example of the late Variscan Salvan-Dorénaz basin (Western Alps). *International Journal of Earth Sciences, 92,* 364–379.

Capuzzo, N., & Wetzel, A. (2004). Facies and basin architecture of the Late Carboniferous Salvan-Dorénaz continental basin (Western Alps, Switzerland/France). *Sedimentology, 51,* 675–697.

Cavin, L., Avanzini, M., Bernardi, M., Piuz, A., Proz, P. A., Meister, Ch., Boissonnas, J., & Meyer, Ch. A. (2012). New vertebrate trackways from the autochthonous cover of the Aiguilles Rouges Massif and reevaluation of the dinosaur record in the Valais (Triassic, SW Switzerland). *Swiss Journal of Palaeontology, 31,* 317–324.

Collet, L.W., Lombard, A, Oulianoff, N., Paréjas, E., & Reinhard, M. (1951). *Geological Atlas of Switzerland 1:25000, No. 24 (Finhaut)*. Wabern: Federal Office of Topography. www.geo.admin.ch.

Corfu, F., Hanchar, J. M., Hoskin, P. W., & Kinny, P. (2003). Atlas of zircon textures. *Reviews in Mineralogy and Geochemistry, 53,* 469–500.

Couzinié, S., Laurent, O., Chelle-Michou, C., Bouilhol, P., Paquette, J. L., Gannoun, A. M., & Moyen, J. F. (2019). Detrital zircon U–Pb–Hf systematics of Ediacaran metasediments from the French Massif Central: Consequences for the crustal evolution of the north Gondwana margin. *Precambrian Research*, *324*, 269–284.

de Graciansky, P. C., Roberts, D., & Tricart, P. (2010). *The Western Alps from rift to passive margin to orogenic belt: an integrated geosciences overview. Developments in Earth surface processes* (Vol. 14). Amsterdam: Elsevier.

Dobmeier, C., Pfeifer, H. R., & von Raumer, J. F. (1999). The newly defined" Greenstone Unit'' of the Aiguilles Rouges massif (western Alps): remnant of an Early Palaeozoic oceanic island-arc? *Schweizerische Mineralogische und Petrographische Mitteilungen, 79,* 263–276.

Fedo, C. M., Sircombe, K. N., & Rainbird, R. H. (2003). Detrital zircon analysis of the sedimentary record. *Reviews in Mineralogy and Geochemistry, 53,* 277–303.

Franke, W. (2000) The mid-European segment of the Variscides: Tectonostratigraphic units, terrane boundaries and plate tectonic evolution, In Franke, W., Haak, V., Oncken, O., & Tanner, D. (Eds.) Orogenic processes: Quantification and modelling in the Variscan Belt: Geological Society of London, Special Publication, 179, 35–61.

Franke, W., Cocks, L. R. M., & Torsvik, T. H. (2017). The Palaeozoic Variscan oceans revisited. *Gondwana Research, 48,* 257–284.

Frey, M., Desmons, J., & Neubauer, F. (1999). Metamorphic maps of the Alps, *Schweizerische*. *Mineralogische und Petrographische Mitteilungen, 79,* 1–230.

Froitzheim, N. (2001). Origin of the Monte Rosa nappe in the Pennine Alps—A new working hypothesis. *Geological Society of America Bulletin, 113,* 604–614.

Garfunkel, Z. (2015). The relations between Gondwana and the adjacent peripheral Cadomian domain—Constrains on the origin, history, and paleogeography of the peripheral domain. *Gondwana Research, 28,* 1257–1281.

Gebauer, D. (1993). The pre-Alpine evolution of the continental crust of the Central Alps—an overview. In J. F. von Raumer & F. Neubauer (Eds.), *Pre-Mesozoic geology in the Alps* (pp. 93–117). Berlin: Springer.

Gehrels, G. (2011). Detrital zircon U–Pb geochronology: Current methods and new opportunities. In C. Busy & A. Azor (Eds.), *Tectonics of sedimentary basins: Recent advances* (pp. 45–62). Chichester: Wiley-Blackwell.

Gerdes, A., & Zeh, A. (2006). Combined U–Pb and Hf isotope LA-(MC-) ICP-MS analysis of detrital zircons: Comparison with SHRIMP and new constraints for the provenance and age of an Armorican metasediment in Central Germany. *Earth and Planetary Science Letters, 249,* 47–61.

Gradstein, F. M., Ogg, J. G., Schmitz, M. D., & Ogg, G. (Eds.). (2012). *The geologic time scale 2012*. Amsterdam: Elsevier.

Grosjean, D. B., Meisser, N., May-Leresche, S., Ulianov, A., & Vonlanthen, P. (2018). The Morcles microgranite (Aiguilles Rouges, Swiss Alps): geochronological and geochemical evidences for a common origin with the Vallorcine intrusion. *Swiss Journal of Geosciences, 111,* 35–49.

Klein, H., Wizevich, M. C., Thüring, B., Marty, D., Thüring, S., Falkingham, P., & Meyer, Ch. A. (2016). Triassic chirotheriid footprints from the Swiss Alps: ichnotaxonomy and depositional environment (Cantons Wallis & Glarus). *Swiss Journal of Palaeontology, 135,* 295–314.

Kroner, U., & Romer, R. L. (2013). Two plates—Many subduction zones: the Variscan orogeny reconsidered. *Gondwana Research, 24,* 298–329.

Kunz, B. E., Manzotti, P., von Niederhäusern, B., Engi, M., Darling, J. R., Giuntoli, F., & Lanari, P. (2018). Permian high-temperature metamorphism in the Western Alps (NW Italy). *International Journal of Earth Sciences, 107,* 203–229.

Linnemann, U., D'Lemos, R., Drost, K., Jeffries, T., Gerdes, A., Romer, R. L., Samson, S. D., & Strachan, R. A. (2008). The Cadomian Orogeny. In T. McCann (Ed.), *The Geology of Central Europe* (pp. 103–154). London: The Geological Society of London.

Linnemann, U., Gerdes, A., Drost, K., & Buschmann, B. (2007). The continuum between Cadomian orogenesis and opening of the Rheic Ocean: Constraints from LA–ICP–MS U–Pb zircon dating and analysis of plate-tectonic setting (Saxo-Thuringian zone, northeastern Bohemian Massif, Germany). In U. Linnemann, R.D. Nance, P. Kraft, & G. Zulauf (Eds.), *The Evolution of the Rheic Ocean: From Avalonian–Cadomian Active Margin to Alleghenian–Variscan Collision*. Geological Society of America Special Paper 423 (pp. 61–96). Boulder: Geological Society of America.

Linnemann, U., Gerdes, A., Hofmann, M., & Marko, L. (2014). The Cadomian Orogen: Neoproterozoic to Early Cambrian crustal growth and orogenic zoning along the periphery of the West African Craton—Constraints from U–Pb zircon ages and Hf isotopes (Schwarzburg Antiform, Germany). *Precambrian Research, 244,* 236–278.

Ludwig, K.R. (2001). Users Manual for Isoplot/Ex rev. 2.49: *Berkeley Geochronology Center Special Publication*, *1a*, 1-56.

Matte, P. (2001). The Variscan collage and orogeny (480–290 Ma) and the tectonic definition of the Armorica microplate: a review. *Terra Nova, 13,* 122–128.

Meinhold, G., Morton, A. C., & Avigad, D. (2013). New insights into peri-Gondwana paleogeography and the Gondwana super-fan system from detrital zircon U–Pb ages. *Gondwana Research, 23,* 661–665.

Meisser, N. (2012). *La minéralogie de l'uranium dans le massif des Aiguilles Rouges (1 carte + 183 p.)*. Wabern: La minéralogie de l'uranium dans le massif des Aiguilles Rouges (1 carte + 183 p.).

Ménot, R. P., Peucat, J. J., Scarenzi, D., & Piboule, M. (1988). 496 My age of plagiogranites in the Chamrousse ophiolite complex (external crystalline massifs in the French Alps): evidence of a Lower Paleozoic oceanization. *Earth and Planetary Science Letters, 88,* 82–92.

Nance, R. D., Gutiérrez-Alonso, G., Keppie, J. D., Linnemann, U., Murphy, J. B., Quesada, C., Strachan, R. A., & Woodcock, N. H. (2010). Evolution of the Rheic ocean. *Gondwana Research, 17,* 194–222.

Nance, R. D., Gutiérrez-Alonso, G., Keppie, J. D., Linnemann, U., Murphy, J. B., Quesada, C., Strachan, R. A., & Woodcock, N. H. (2012). A brief history of the Rheic Ocean. *Geoscience Frontiers, 3,* 125–135.

Paquette, J. L., Menot, R. P., & Peucat, J. J. (1989). REE, Sm–Nd and U–Pb zircon study of eclogites from the Alpine External Massifs (Western Alps): evidence for crustal contamination. *Earth and Planetary Science Letters, 96,* 181–198.

Potrel, A., Peucat, J. J., Fanning, C. M., Auvray, B., Burg, J. P., & Caruba, C. (1996). 3.5 Ga old terranes in the West African craton, Mauritania. *Journal of the Geological Society, 153,* 507–510.

Ring, U., Collins, A. S., & Kassem, O. K. (2005). U–Pb SHRIMP data on the crystallization age of the Gran Paradiso augengneiss, Italian Western Alps: Further evidence for Permian magmatic activity in the Alps during break-up of Pangea. *Eclogae Geologicae Helvetiae, 98,* 363–370.

Robardet, M. (2003). The Armorica 'microplate': fact or fiction? Critical review of the concept and contradictory palaeobiogeographical data. *Palaeogeography, Palaeoclimatology, Palaeoecology, 195,* 125–148.

Romer, R. L., & Kroner, U. (2019). First direct evidence for a contiguous Gondwana shelf to the south of the Rheic Ocean. *Geology*, *47*, 767–770. https://doi.org/10.1130/G46255.1.

Rösel, D., Boger, S. D., Möller, A., Gaitzsch, B., Barth, M., Oalmann, J., & Zack, T. (2014). Indo-Antarctic derived detritus on the northern margin of Gondwana: evidence for continental-scale sediment transport. *Terra Nova, 26,* 64–71.

Schaltegger, U. (1993). The evolution of the polymetamorphic basement in the Central Alps unravelled by precise U−Pb zircon dating. *Contributions to Mineralogy and Petrology, 113,* 466–478.

Schaltegger, U. (1994). Unravelling the pre-Mesozoic history of Aar and Gotthard massifs (Central Alps) by isotopic dating: a review: The pre-Alpine crustal evolution of the Aar-, Gotthard-and Tavetsch massifs. *Schweizerische Mineralogische und Petrographische Mitteilungen, 74,* 41–51.

Schaltegger, U., Abrecht, J., & Corfu, F. (2003). The Ordovician orogeny in the Alpine basement: constraints from geochronology and geochemistry in the Aar Massif (Central Alps). *Schweizerische Mineralogische und Petrographische Mitteilungen, 83,* 183–239.

Schaltegger, U., & Corfu, F. (1995). Late Variscan "Basin and Range" magmatism and tectonics in the Central Alps: evidence from U–Pb geochronology. *Geodinamica Acta, 8,* 82–98.

Schaltegger, U., & Gebauer, D. (1999). Pre-Alpine geochronology of the Central, Western and Southern Alps. *Schweizerische Mineralogische und Petrographische Mitteilungen, 79,* 79–87.

Scheck-Wenderoth, M., Krzywiec, P., Zühlke, R., Maystrenko, Y., & Froitzheim, N. (2008). Permian to Cretaceous tectonics. In T. McCann (Ed.), *The geology of Central Europe* (Vol. 2, pp. 999–1030). London: The Geological Society of London.

Schmid, S. M., Pfiffner, O. A., Froitzheim, N., Schönborn, G., & Kissling, E. (1996). Geophysical-geological transect and tectonic evolution of the Swiss-Italian Alps. *Tectonics, 15,* 1036–1064.

Schulz, B., & von Raumer, J. F. (2011). Discovery of Ordovician-Silurian metamorphic monazite in garnet metapelites of the Alpine External Aiguilles Rouges Massif. *Swiss Journal of Geosciences, 104,* 67–79.

Schuster, R., & Stüwe, K. (2008). Permian metamorphic event in the Alps. *Geology, 36,* 603–606.

Siegesmund, S., Oriolo, S., Heinrichs, T., Basei, M. A. S., Nolte, N., Hüttenrauch, F., & Schulz, B. (2018). Provenance of Austroalpine basement metasediments: tightening up Early Palaeozoic connections between peri-Gondwanan domains of central Europe and Northern Africa. *International Journal of Earth Sciences, 107,* 2293–2315.

Simon-Coinçon, R. (1999). Palaeolandscape Reconstruction of the South-Western Massif Central (France). In M. Thiry & R. Simon-Coinçon (Eds.), *Palaeoweathering, Palaeosurfaces and Related Continental Deposits*, vol. 27 (pp. 223–243). International Association of Sedimentologists, Oxford: Blackwell Science.

Sircombe, K. N. (2004). AGE DISPLAY: an EXCEL workbook to evaluate and display univariate geochronological data using binned frequency histograms and probability density distributions. *Computers & Geosciences, 30,* 21–31.

Stacey, J. S., & Kramers, J. D. (1975). Approximation of terrestrial lead isotope evolution by a two-stage model. *Earth and Planetary Science Letters, 26,* 207–221.

Stampfli, G. M., & Borel, G. D. (2002). A plate tectonic model for the Paleozoic and Mesozoic constrained by dynamic plate boundaries and restored synthetic oceanic isochrons. *Earth and Planetary Science Letters, 19,* 17–33.

Stampfli, G. M., Borel, G. D., Marchant, R., & Mosar, J. (2002). Western Alps geological constraints on western Tethyan reconstructions. *Journal of the Virtual Explorer, 7,* 75–104.

Stampfli, G. M., & Hochard, C. (2009). Plate tectonics of the Alpine realm. In J. B. Murphy, J. D. Keppie, & A. J. Hynes (Eds.), *Ancient orogens and modern analogues* (Vol. 327, pp. 89–111). London: Geological Society, Special Publications. https://doi.org/10.1144/SP327.6.

Stampfli, G. M., Hochard, C., Vérard, C., & Wilhem, C. (2013). The formation of Pangea. *Tectonophysics, 593,* 1–19.

Stampfli, G. M., von Raumer, J., & Wilhem, C. (2011). The distribution of Gondwana-derived terranes in the Early Palaeozoic. In J. C. Gutiérrez-Marco, I. Rabano, & D. García-Bellido (Eds.), *Ordovician of the World* (pp. 567–574). Madrid: Instituto Geológico y Minero de España.

Stephan, T., Kroner, U., & Romer, R. L. (2019a). The pre-orogenic detrital zircon record of the Peri-Gondwanan crust. *Geological Magazine, 156,* 281–307.

Stephan, T., Kroner, U., Romer, R. L., & Rösel, D. (2019b). From a bipartite Gondwana shelf to an arcuate Variscan belt: The early Paleozoic evolution of northern Peri-Gondwana. *Earth-Science Reviews, 192,* 491–512.

Thomas, W. A. (2011). *Detrital-zircon geochronology and sedimentary provenance. Lithosphere, 3,* 304–308.

von Raumer, J. F. (1969). Stilpnomelan als alpinmetamorphes Produkt im Mont-Blanc-Granit. *Contributions of Mineralogy and Petrology, 21,* 257–271.

von Raumer, J. F. (1974). Zur Metamorphose amphibolititscher Gesteine im Altkristallin des Mon-Blanc- und Aiguilles-Rouges-Massivs. *Schweizerische Mineralogische und Petrographische Mitteilungen, 54,* 471–488.

von Raumer, J. F. (1998). The Palaeozoic evolution in the Alps: from Gondwana to Pangea. *Geologische Rundschau, 87,* 407–435.

von Raumer, J., Abrecht, J., Bussy, F., Lombardo, B., Menot, R. P., & Schaltegger, U. (1999). The Paleozoic metamorphic evolution of the Alpine external massifs. *Schweizerische Mineralogische und Petrographische Mitteilungen, 79,* 5–22.

von Raumer, J. F., & Bussy, F. (2004). Mont Blanc and Aiguilles Rouges: Geology of their Polymetamorphic basement (External Massifs, Western Alps, France-Switzerland). *Mémoires de Géologie (Lausanne), 42,* 1–203.

von Raumer, J. F., Bussy, F., Schaltegger, U., Schulz, B., & Stampfli, G. M. (2013). Pre-Mesozoic Alpine basements—their place in the European Paleozoic framework. *Geological Society of America Bulletin, 125,* 89–108.

von Raumer, J. F., Bussy, F., & Stampfli, G. M. (2009). The Variscan evolution in the External massifs of the Alps and place in their Variscan framework. *Comptes Rendus Geoscience, 341,* 239–252.

von Raumer, J. F., & Stampfli, G. (2008). The birth of the Rheic Ocean—Early Palaeozoic subsidence patterns and subsequent tectonic plate scenarios. *Tectonophysics, 461,* 9–20.

von Raumer, J. F., Stampfli, G., Borel, G., & Bussy, F. (2002). Organization of pre-Variscan basement areas at the north-Gondwanan margin. *International Journal of Earth Sciences, 91,* 35–52.

Wizevich, M. C., Ahern, J., & Meyer, Ch A. (2019). The Triassic of southwestern Switzerland—Marine or not marine, that is the question! *Palaeogeography, Palaeoclimatology, Palaeoecology, 514,* 577–592.

Žák, J., & Sláma, J. (2018). How far did the Cadomian 'terranes' travel from Gondwana during early Palaeozoic? A critical reappraisal based on detrital zircon geochronology. *International Geology Review, 60,* 319–338.

Ziegler, P. A. (1982). Triassic rifts and facies patterns in Western and Central Europe. *Geologische Rundschau, 71,* 747–772.